Nanoscale

ROYAL SOCIETY OF CHEMISTRY

COMMUNICATION

View Article Online
View Journal | View Issue

Cite this: *Nanoscale*, 2025, **17**, 6448

Received 29th October 2024,
Accepted 3rd February 2025

DOI: 10.1039/d4nr04507f

rsc.li/nanoscale

Slippery liquid-like surfaces as a promising solution for sustainable drag reduction†

Lingxuan Hao and Bei Fan *

Drag reduction is crucial for many industries, ranging from aerospace to microfluidics, to enhance the energy efficiency and reduce costs. This work is the first to study drag reduction enabled by novel slippery liquid-like surfaces fabricated from flexible polymers. We experimentally characterized the drag reduction performance of slippery liquid-like surfaces in the laminar flow regime. Our results indicate that liquid-like surfaces can reduce fluid drag regardless of surface wettability and have achieved nearly 20% drag reduction. Furthermore, the durability tests show that these surfaces can maintain slipperiness over a month when exposed to air or water and the drag reduction capability for at least one week under a fluid flow. These findings highlight the potential of slippery liquid-like surfaces as a promising solution for sustainable drag reduction.

Department of Mechanical Engineering, Michigan State University, East Lansing, MI, 48823, USA. E-mail: fanbei1@msu.edu

†Electronic supplementary information (ESI) available. See DOI: https://doi.org/10.1039/d4nr04507f

Bei Fan

Dr Bei Fan received her Ph. D in Mechanical Engineering from the University of California San Diego in 2019 and completed her postdoc at Lawrence Berkeley National Laboratory in 2021. Then, she joined Mechanical Engineering at Michigan State University in 2021. Her research interests cover broad areas including thermal fluid science, microfluidic devices, electrokinetics, energy conversion and harvesting, desalination, and micro/nano-fabrication. Her work has been published in high-reputation journals such as Science Advances, Nature Communications, Langmuir and Applied Physics Letters and reported by public media including Science Daily, Phys.org, Physics Today, etc. She was awarded with NSF grant awards.

1. Introduction

Drag reduction plays key roles in various engineering and industrial applications, particularly in the petroleum industry,[1,2] aerospace engineering,[3,4] microfluidic devices,[5,6] liquid cooling systems,[7,8] and marine transportation.[9,10] Reducing the flow drag not only improves the energy efficiency, but also increases the overall performance and lifespan of systems by minimizing friction between fluid and solid surfaces, for example in underwater vehicles,[11] aviation,[2] pipeline transportation,[12] wind turbine blade design,[13] automotive aerodynamics,[3] and droplet manipulation[14–24] where fluid flow resistance can lead to significant energy losses. Effective drag reduction strategies can lead to substantial cost savings and environmental benefits. In microfluidics, drag reduction can improve the pumping efficiency and achieve higher throughput[25] during DNA analysis,[26] cell sorting[27] and blood diagnosis,[28] as well as limiting shear damage, aggregation and sedimentation in medical flows.[29]

Surface engineering has been widely employed to reduce drag by generating fluid slip at the fluid–surface interface.[30,31] When the fluid flows over a solid surface, the no-slip boundary condition (zero flow velocity at the fluid–solid interface) is generally applied. However, if fluid slip appears at the interfaces, as shown in Fig. 1(a), the Navier slip boundary condition is applicable. This condition states that the slip velocity (the flow velocity along the streamwise direction at the slipping interface) is proportional to the rate of strain at the interface. Mathematically, it can be expressed as:

$$u_{\text{slip}} = b\frac{\partial u}{\partial y}|_{\text{w}} \tag{1}$$

where u_{slip} is the slip velocity, b is the slip length (up to the order of μm), and $\frac{\partial u}{\partial y}|_{\text{w}}$ is the shear rate at the wall. In existing

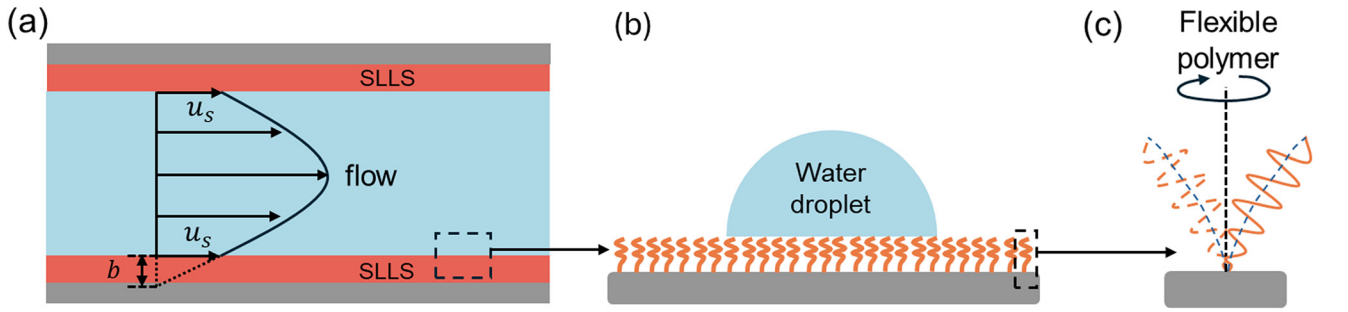

Fig. 1 (a) The schematic of a microchannel with slippery liquid-like surfaces (SLLSs) as the channel surfaces. When liquid is running through the microchannel, a fluid slip will be induced at the liquid–SLLS interface. The μ_s is the fluid slip velocity at the liquid–SLLS interface, and b is the slip length which is the extended length to which the fluid velocity vanishes. (b) Zoom-in image of the SLLS made by grafting (c) flexible polymers to a substrate.

studies, various surface treatments and coatings have been developed to induce fluid slip for drag reduction. For example, superhydrophobic surfaces[32–34] (SHSs) utilize micro/nanostructures and low surface energy materials to trap air when the liquid flows over them. The liquid is in contact with solids only at the peaks of the micro/nanostructures, while the rest of the surface is exposed to air, which has nearly zero viscosity. The configuration enables the liquid to move over the trapped air with significantly reduced friction, creating apparent fluid slip at liquid–air interfaces.[33,35–39] Benefiting from the ultra-low viscosity of air, SHSs can achieve high drag reduction performance. Lee *et al.* summarized experimental slip measurement on SHSs and reported 5%–60% drag reduction performance.[40] However, the air–liquid interface of SHSs will break up and result in the loss of trapped air under increased external pressure.[41] In addition, while the hydrostatic pressure and water flow rate increase, the dissolution ability of air in water will increase due to the mass transfer forced convection.[42] Therefore, SHSs often fail to maintain the fluid slip due to the air depletion under a liquid flow. For example, Xiang *et al.* demonstrated that SHSs lost non-wettability after 30 minutes under a liquid flow.[43] To restore the slipperiness of SHSs, various methods for regenerating the trapped air in SHSs have been proposed, including *in situ* gas generation *via* water decomposition, heating, and gas injection through gas permeable base materials. For instance, Lloyd *et al.* demonstrated an electrochemical controlling strategy to replenish hydrogen from water decomposition.[44] Saranndhi *et al.* regenerated the plastron of SHSs by activated heating of SHSs to establish the Leidenfrost state at a relatively low superheat temperature.[45] Breveleri *et al.* restored the plastron in 0.3 seconds by injecting a high-pressure gas from the bottom of a porous material.[46] Similarly, Zhao *et al.* injected bubbles to recover the plastron by utilizing the sparse nanostructure with low surface energy.[47] Nevertheless, these active methods for enhancing the stability of SHSs increase the complexity level of operation and make SHSs not suitable in certain applications, such as microfluidic electrokinetic energy conversion devices. Besides, slippery liquid-infused porous surfaces[48] (SLIPSs) have been designed to mimic the slipperiness of natural surfaces, such as Nepenthes pitcher plants, by infusing liquid lubricants into the surface structures. An immiscible liquid can move over the lubricant layer with a significant fluid slip.[49–53] Studies reported that SLIPSs can achieve 7%–50% drag reduction by optimizing the surface structure design and infused liquid lubricant.[5] Despite their effectiveness, SLIPSs suffer from lubricant loss due to shear force under a fluid flow and would fail within minutes to 24 hours under a flow.[54–59] The lack of robustness has historically impeded the successful implementation of SHSs and SLIPSs.

Recently, a novel type of slippery liquid-like surface has been developed by grafting flexible polymers onto substrates.[60–66] These surfaces exhibited several unique properties. First, slippery liquid-like surfaces have flexible polymers that behave like a liquid lubricant layer as shown in Fig. 1(b) and (c). Zhao *et al.* reported the macroscopic evidence of the Couette-like flow behavior of flexible polymers under shear with an effective viscosity,[67] which enables slippery liquid-like surfaces to induce fluid slip when liquids flow over them. Second, slippery liquid-like surfaces have excellent liquid repellency. These surfaces can repel liquids with various surface tensions and contact angles. As flexible polymers behave like a liquid lubrication layer, the friction between the surface and liquids in contact is greatly reduced. Wang and McCarthy *et al.* reported that slippery liquid-like surfaces show ultralow contact angle hysteresis (CAH < 1°).[66] Zhang *et al.* also reported that slippery liquid-like surfaces show negligible contact angle hysteresis (CAH < 1.5°) to water and highly wetting liquids, *e.g.* FC72 (γ = 10 mN m^{-1}), Krytox 101(γ = 17 mN m^{-1}), and hydrocarbon oils.[63] Lastly, slippery liquid-like surfaces also have shown exceptional durability. By circumventing the use of fragile micro/nano-textures and air/liquid lubricants, the non-textured all-solid features of slippery liquid-like surfaces mitigate the mechanical damage and loss of the lubricant. Zhang *et al.*[63] showed that slippery liquid-like surfaces remained durable even after 1000 cycles of mechanical abrasion/adhesion tests and scratch damage, while the SLIPSs lost the liquid repellency in the same test. Evidently, slippery liquid-like surfaces have the potential to solve the long-standing durability issue associated with SHSs and SLIPSs for sustainable drag reduction benefiting from the

abovementioned unique properties. Despite these advantages, there is little work on drag reduction over slippery liquid-like surfaces. Currently, most studies still focus on liquid-repellency,[68,69] anti-icing,[62,70–74] anti-fouling,[75,76] and enhanced condensation[77,78] enabled by slippery liquid-like surfaces. Thus, this work is the first to experimentally characterize the drag reduction performance and durability of SLLSs under a liquid flow.

In this study, we experimentally quantified the drag reduction enabled by both hydrophobic and hydrophilic slippery liquid-like surfaces at different flow rates and Reynolds numbers within the laminar flow regime. We also tested the durability of slippery liquid-like surfaces under hydrostatic pressure and hydrodynamic flow conditions. Our results demonstrated that slippery liquid-like surfaces could induce drag reduction regardless of their wettability. The tested surfaces have generated effective drag reduction in the range of 6.4%–21.1%. Moreover, slippery liquid-like surfaces have shown remarkable durability, especially the hydrophilic one has maintained its drag reduction capability for at least one week under a continuous flow.

2. Methods

2.1. Liquid-like surface fabrication

2.1.1. Hydrophobic slippery liquid-like surface. We fabricated the hydrophobic slippery liquid-like surface by grafting chlorine-terminated poly(dimethylsiloxane) (Gelest Inc.) polymer brushes onto a silicon (Si) substrate with the vapor deposition approach.[60] The Si substrate was pre-cleaned with acetone, isotropy alcohol (IPA), and deionized (DI) water and dried with an air nozzle subsequently. Then, a 20 minute oxygen-based plasma treatment was applied to the Si substrate to clean the substrate and create hydroxyl groups. The plasma treated surface was then placed upside down on the cover of a Petri dish, containing 800 μL of liquid chlorine-terminated with the corresponding molar weight (425 g mol^{-1}) which is denoted as V_425 below. The assembled Petri dish was placed in a vacuum oven at 60 °C for 1 hour. Finally, the substrates were rinsed in a toluene bath in an ultrasonic shaker for 2 min, cleaned with acetone, IPA, and DI water sequentially to remove untethered residue chemicals and dried with an air nozzle.

2.1.2. Hydrophilic slippery liquid-like surface. We fabricated the hydrophilic liquid-like surface[64] by covalently grafting polyethylene glycol (PEG) brushes to bare Si substrates. The Si substrates were cleaned with acetone and DI water and then dried in air. The cleaned surfaces were exposed to oxygen plasma for 10 minutes for hydroxylation. The hydroxylated substrates were then immersed in a mixture of solution consisting of 2 μL of 2-methoxy polyethyleneoxy (6–9) propyl trimethoxysilane (Gelest Inc.), 12 μL of hydrochloric acid (Fisher Inc.), and 45 mL of toluene (Sigma-Aldrich) in a glass Petri dish. Finally, the grafted samples were rinsed in a toluene bath for 2 minutes in an ultrasonic shaker and cleaned with DI water and ethanol (Sigma-Aldrich) sequentially and dried in air.

2.2. Surface characterization

The wetting properties of a surface consist of contact angle (CA), contact angle hysteresis (CAH), and sliding angle (SA). The CA was measured by depositing 5 μL DI water droplets onto flat testing surfaces using an automated dispenser and a goniometer (Rame-hart 290) at room temperature under ambient conditions. The test surface was positioned horizontally. A 5 μL DI droplet was first dispensed very slowly to avoid splashing or irregular shape formation. Then, the droplet was placed on the testing surface and the dispenser was carefully removed. A slight vibration (*i.e.*, expansion and contraction) of the droplet was initially observed after the droplet was placed onto the testing surface. Once there was no obvious vibration of the droplet, the representative CA was quickly measured 10 times to mitigate the effects of droplet evaporation. The representative CA is the value by averaging the 10 readings of the contact angles at the left and right edges. This process was repeated at three independent positions on the same testing surface to check the variation in wetting properties on the surface. (The CA at the left and right edges are provided in ESI S2.1.†) The CAH was measured by tilting the surface slowly with 0.3 degrees per s until the droplet started sliding on the surface.[79] The angle at which the surface was tilted was the SA. The difference between the contact angle at the advancing edge (θ_{adv}) and the receding edge (θ_{rec}) is defined as CAH. All CAH and SA measurements were obtained on 3 independent positions on each surface. The surface roughness was measured by atomic force microscopy (AFM) with a tapping mode. The surface morphology was examined with scanning electric microscopy (SEM) (see ESI S1†). The coating thickness was analyzed with an ellipsometer at a 70-degree inclined angle with a He–Ne laser (λ = 900 nm). The Cauchy model was applied to calculate the thickness of the polymer brush layer. The polymer brush layer thickness measurements are also obtained on 3 different positions on the surfaces.

2.3. Drag reduction measurement

Pressure drop measurement in a microchannel is a standard method to quantify the drag reduction for engineered surfaces.[80] We designed a 3-layer sandwich structured microchannel to perform drag reduction measurement. As shown in Fig. 2, the top polycarbonate plane and the bottom test surface are separated using a silicone rubber sheet (thickness = 0.005″, McMaster-Carr). A rectangular shape (length = 76.5 mm, width = 10 mm) was cut at the center of the rubber sheet to define the microchannel shape and dimensions. In a flow experiment, the DI water was pumped through a microchannel using a syringe pump (Havard Apparatus Pump 11 Elite) using 5 controlled flow rates of 20, 22.5, 25, 27.5, and 30 mL min^{-1}. A differential pressure sensor with a high accuracy of 2 Pa (Omega Engineering PX459-10WDWU5 V) was used to measure the pressure drop across the microchannel. The drag reduction measurement was performed fifteen times at each flow rate and the average value of all measurements was used (see ESI S4†). Because the channel height slightly

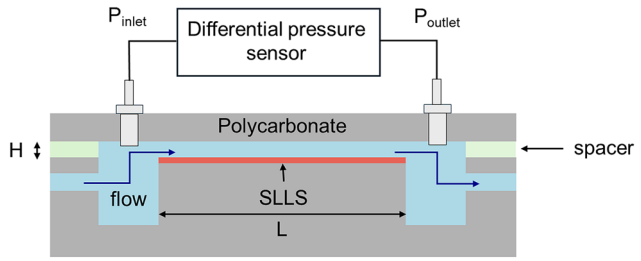

Fig. 2 Schematic of the drag reduction measurement setup (assembling details see ESI Fig. S3†). The top polycarbonate plate and testing slippery liquid-like surface (SLLS) are separated by a thin silicone rubber spacer. The microchannel has dimensions with length L = 76.5 mm and width W = 10 mm. In drag reduction measurement, water was pumped through the microchannel at controlled flow rates using a syringe pump. The differential pressure sensor was pumped through the microchannel at controlled flow rates using a syringe pump. The differential pressure sensor was connected to the ports in the inlet and outlet reservoirs to measure the pressure drop across the microchannel.

changes for each assembled microfluid channel, the channel height for each experiment was also measured independently. To accurately determine the channel height, after the flow experiment of each test surface, liquid silicone rubber (Ecoflex 00-50) was injected into the microchannel without opening the microchannel.[59] After 12 hours of curing, the solidified silicone rubber was removed from the disassembled microchannel device. The thickness of the silicone rubber was measured at three independent positions with a digital profilometer (Keyence, VHX-6000).

2.4. Durability test

2.4.1. Durability test under hydrostatic pressure. To test the durability of slippery liquid-like surfaces under hydrostatic pressure, one set of surfaces was exposed to air and another set of surfaces was immersed in DI water for 30 days. The wetting properties (*i.e.*, CA, CAH, and SA values) were characterized every day on 3 different positions respectively using a goniometer. We also examined the durability of slippery liquid-like surfaces in acidic and alkaline solutions by immersing each surface in solutions with different pH values (pH = 1, 4, 10, 13) (see ESI S7†).

2.4.2. Durability test under a hydrodynamic flow. To test the durability of slippery liquid-like surfaces under hydrodynamic flow, we connected the assembled microchannel with a circular pump and used a flow rate of 20 mL min^{-1} to continuously pump water flows over slippery liquid-like surfaces for one week or until the surface failed (depending on which comes earlier). The pressure across the microchannel was measured four times every day.

3. Results and discussion

3.1. Surface slipperiness and drag reduction performance

Table 1 and Fig. 3 show the surface characterization results. As shown in Table 1 and Fig. 3(a) and (d), the hydrophobic liquid-like surface has a CA of around 104.7° and the hydrophilic liquid-like surface has a CA of around 42.2°. Both hydrophobic and hydrophilic liquid-like surfaces show exceptional slipperiness from their ultra-low CAH and SA values as shown in Fig. 3(b) and (e). The standard deviation values presented in Table 1 indicate the degree of variation in the measured CA and CAH values across different positions and readings. These values demonstrate that the observed uncertainties and potential experimental errors are minimal, ensuring the reliability and reproducibility of the measurements. (All measured advancing angles and receding angles at three positions are provided in ESI S2.2.†) The ultra-low CAH of the slippery liquid-like surface is a result of its low physical and chemical inhomogeneities.[64] From the AFM measurement in Fig. 3(c) and (f), liquid-like surfaces are ultra-smooth, which induces low physical inhomogeneity. Additionally, the liquid-like surface fabrication methods we employed from the literature[60,65] will lead to a high grafting density that also gives low chemical inhomogeneity.[64]

Table 1 Surface characterization results of the fabricated slippery liquid-like surfaces

	V_425	PEG
CA (°)	104.7 ± 0.5	42.2 ± 2.3
SA (°)	5.6 ± 1.7	6.5 ± 0.4
Advancing angle (°)	105.6 ± 0.4	43.8 ± 2.3
Receding angle (°)	104.0 ± 0.5	42.0 ± 2.3
CAH (°)	1.5 ± 0.5	1.7 ± 0.4
Thickness (nm)	6.5	22.0
Roughness (nm)	2.14	0.81

The pressure drop across the microchannel was measured to determine the drag reduction performance of the test surface. For a solid surface with the no-slip boundary condition, in the laminar flow regime, the measured pressure drop (ΔP_{no_slip}) will follow the theoretical value of the Poiseuille flow:

$$\Delta P_{no\_slip} = \frac{12\mu LQ}{WH^3} \quad (2)$$

where Q represents the flow rate in the microchannel; L, W, and H denote the microchannel length, width, and height, respectively; and μ is the dynamic viscosity of DI water which is about 0.001 Pa s.[81] We first validated the accuracy of our experiment setup by measuring the pressure drop when water flowed over a smooth Si surface which functioned as the reference no-slip surface. The measured results showed no drag reduction on the smooth Si surface (see ESI S5†).

When fluid slip appears at the test surfaces, the measured pressure drop ΔP_{slip} is expected to be lower than ΔP_{no_slip} at the no-slip condition. The drag reduction (DR) coefficient of the test surface can be calculated from:[59]

$$DR = \frac{\Delta P_{no\_slip} - \Delta P_{slip}}{\Delta P_{no\_slip}} \quad (3)$$

Fig. 4 shows the experimental results of pressure drop using different flow rates for hydrophobic (V_425) and hydro-

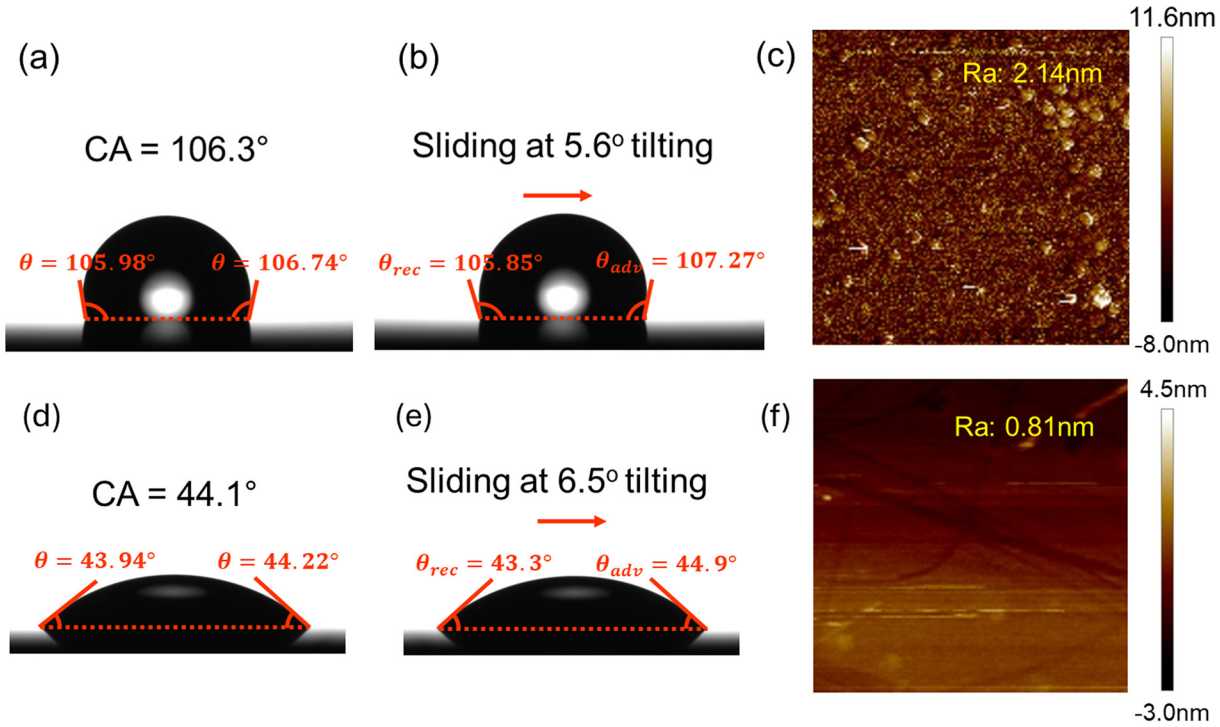

Fig. 3 (a)–(c) present the single measurement of CA, CAH and SA values and the AFM roughness measurement on a 3 μm × 3 μm area for the hydrophobic slippery liquid-like surface. (d)–(f) show the single measurement of CA, CAH and SA values and the AFM roughness measurement using a 3 μm × 3 μm area for the hydrophilic slippery liquid-like surface.

philic (PEG) slippery liquid-like surfaces. The pressure drop approximately increased linearly with the applied flow rate. As illustrated in Fig. 4, for both hydrophobic and hydrophilic slippery liquid-like surfaces, the experimentally measured pressure drop values are smaller than $\Delta P_{\text{no\_slip}}$. This suggests that both surfaces can reduce the pressure drop across the microchannel at a fixed flow rate and induce drag reduction.

From the pressure drop measurements in Fig. 4, we can obtain the dependence of the drag reduction (DR) coefficient on the flow Reynolds number (Re), which is shown in Fig. 5. Re for a rectangular microchannel is defined as:

$$\mathrm{Re} = \frac{UD_{\mathrm{h}}}{\nu} \tag{4}$$

where U is the average flow velocity, ν is the kinematic viscosity of the fluid (*i.e.*, water in our experiment), and $D_{\mathrm{h}} = 2W \times H/(W + H)$ is the hydraulic diameter of a rectangular channel.

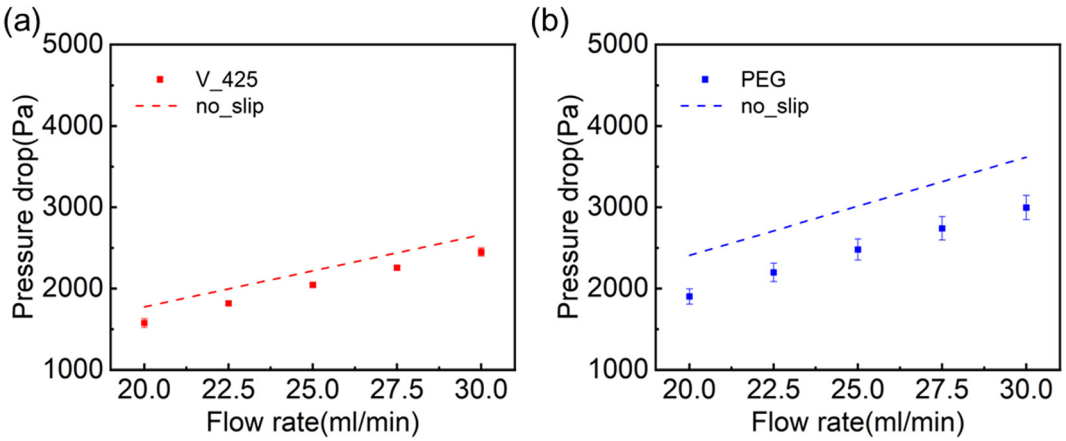

Fig. 4 Shows the pressure drop measurements for both (a) hydrophobic (V_425) and (b) hydrophilic (PEG) slippery liquid-like surfaces at different flow rates. The dots represent the experimental results, while the dashed lines represent the theoretical pressure values at the no-slip boundary condition.

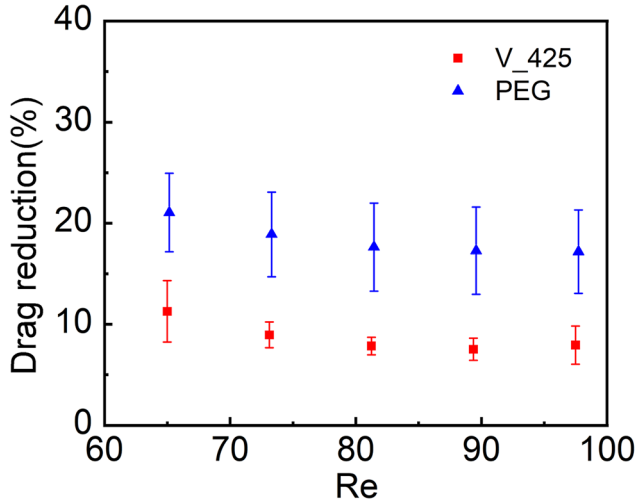

Fig. 5 Drag reduction coefficients at different Re numbers for slippery liquid-like surfaces.

As illustrated in Fig. 5, the hydrophilic liquid-like surface (PEG) has achieved a DR coefficient in the range of 17.2%–21.1%, while the hydrophobic liquid-like surface (V_425) has achieved a DR coefficient in the range of 6.4%–10.2%. The measured drag reduction performance of the slippery liquid-like surfaces could be comparable to those of SHSs (DR coefficient[40,82,83] is 5%–60%) and SLIPSs (DR coefficient[5,48] is 7%–50%). These results also demonstrated that slippery liquid-like surfaces could induce drag reduction regardless of their wettability. This is mainly because the key to generating drag reduction is the presence of a slipping interface. As the slippery liquid-like surfaces behave like a liquid lubricant under shear,[67] a slipping liquid-like/liquid interface will be created once water flows over these surfaces. Thus, both hydrophobic and hydrophilic slippery liquid-like surfaces can achieve drag reduction. It is also noteworthy that the DR coefficient slightly decreased as the Re number (or flow rate) increased. The fluid slip at a slipping interface is $b \sim \frac{\mu_f}{\mu_l} h_0$ (where μ_f is the flowing fluid dynamic viscosity, μ_l is the fluid lubricant dynamic viscosity, and h_0 is the lubricant layer thickness). According to Zhao *et al.*, the apparent viscosity of the slippery liquid-like surface slightly decreases with increasing shear rate.[67] Therefore, μ_l of the liquid-like lubricant layer will decrease slightly when the flow rate (*i.e.*, Re that is varied by changing the flow rate in our experiment) increases. However, at the same time, the larger shear rate at a higher applied flow rate will cause a higher degree of deformation or bending of the flexible polymers, thus reducing the effective lubrication layer thickness h_0. Combining both the effects of μ_l and h_0, the reason for the slightly reduced DR coefficient at a higher Re (or flow rate) could be the domination of reduction in h_0 over the decrease of μ_l when increasing the shear rate in our current applied range. Due to the competing effect between μ_l and h_0 on the fluid slip, we also suspect that there could exist an optimal shear rate at which the DR coefficient reaches the maximum value, which will be tested in a future study. Furthermore, the higher DR coefficient achieved by the hydrophilic liquid-like surface compared to that of the hydrophobic one could be due to its higher coating thickness or h_0 which will lead to a larger fluid slip.

3.2. Exceptional durability of liquid-like surfaces

In the air environment of the hydrostatic pressure durability test, as shown in Fig. 6(a)–(c), the hydrophobic liquid-like surface remained hydrophobic and its slipperiness after 30 days. For the hydrophilic liquid-like surface, although its CA value started rising after 20 days (but still being hydrophilic), the surface still had low SA and CAH after 30 days and sustained good slipperiness. In the DI water environment, as shown in Fig. 6(d)–(f), the hydrophilic liquid-like surface kept its hydrophilicity and slipperiness after 30 days. For the hydrophobic liquid-like surface, the CA decreased but the surface still had good slipperiness based on its low CAH and SA. The hydrostatic pressure durability testing results demonstrated that the slippery liquid-like surface could sustain its slipperiness for at least 30 days in both air and liquid environments. We also assessed the acidic and alkaline resistance on slippery liquid-like surfaces (see ESI S7† for the testing results). Both hydrophobic and hydrophilic slippery liquid-like surfaces can maintain the surface wetting properties for over hundreds of hours in relatively weak acid (pH = 4) and base (pH = 10) solutions but fail within a couple of hours in strong acid (pH = 1) and base (pH = 13) solutions. In general, the PEG surface demonstrated higher resistance in an acidic environment, and the V_425 surface exhibited higher resistance in a base environment.

The adhesion of foulants, such as dust, organic oil and biomolecules, can lead to the loss of original surface properties.[76] For example, some smooth surfaces, such as metal and rare earth oxides, can transition from being hydrophilic to hydrophobic due to the adsorption of organic contaminants presenting in the air within 4 days.[84] To mitigate this contamination, a clean storage strategy utilizing ultraclean nanotextured storage media as a getter has been proposed.[85] The proposed storage device can maintain surface cleanliness for more than 1 week and passively clean contamination on the sample.[85] Remarkably, slippery liquid-like surfaces have been reported to reduce the adhesion of various contaminations in previous studies. For instance, Dai *et al.* obtained ultra-low CAH with Krytox101 (CAH = 0.5°), FC40 (CAH = 0.4°), and FC72 (CAH = 0.2°) droplets on slippery liquid-like surfaces, which indicated high repellency to various organic oils.[61] Besides, our static durability test results in air, as shown in Fig. 6(a)–(c), further confirm that the hydrophobic slippery liquid-like surfaces remained hydrophobic and maintained their slipperiness after 30 days. For hydrophilic slippery liquid-like surfaces, although its CA value started rising after 20 days (but still being hydrophilic), the surface still had a low SA and CAH after 30 days and sustained good slipperiness. The results indicated that both slippery liquid-like surfaces can maintain wettability and slipperiness in the air environment for a long time, which demonstrates mitigated adsorption of organic contamination

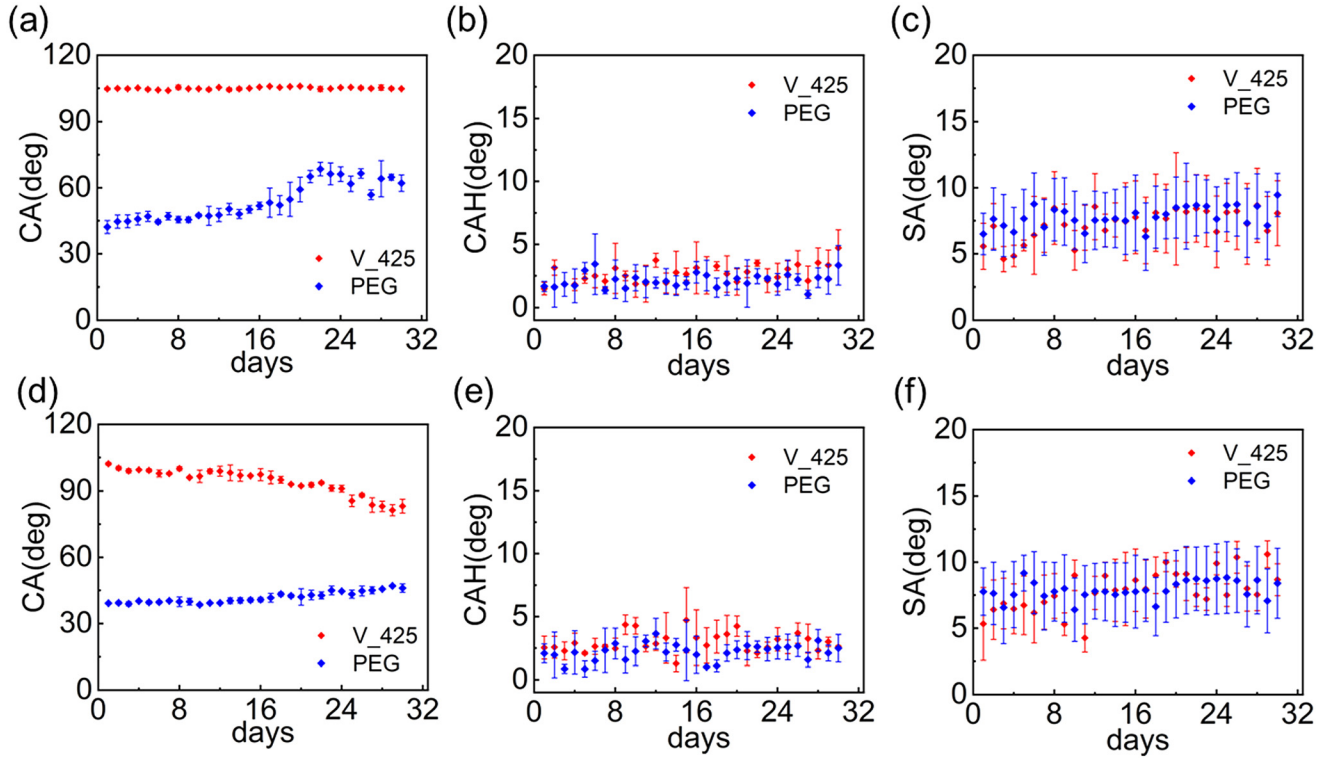

Fig. 6 (a)–(c) Change in the wetting properties *i.e.*, CA, CAH, and SA, of slippery liquid-like surfaces with time while exposed in an air environment; (d)–(f) change in wetting properties, *i.e.*, CA, CAH, and SA, of the slippery liquid-like surface while being immersed in DI water.

in air. Furthermore, Peng *et al.* embedded PDMS chains into the fluorinated ethylene-(hydroxyl-alkyl) vinyl ether (FEVE) matrix to develop solar cells with self-cleaning properties, addressing the issue of dust contamination.[86] Their group also presented exceptional biofilm suppression, such as bacterial cells, on hydrophobic slippery liquid-like surfaces.[87]

Fig. 7 shows the results of the durability test under a hydrodynamic flow. When the surface loses its drag reduction capability, the pressure drop will increase significantly compared to the initial value. From the testing results in Fig. 7, the hydrophobic liquid-like surface (V_425) could keep its drag reduction capability for 56 hours at which its DR coefficient reduced from 9% to 0%. Remarkably, the hydrophilic liquid-like surface (PEG) could still achieve 10% after 160 hours (one-week continuous flow, initial DR coefficient = 19%). In contrast, the SHSs would lose their slipperiness after 30 minutes under a liquid flow[43] and SLIPSs lost the drag reduction capability after 14 minutes or 24 hours under laminar flow in a

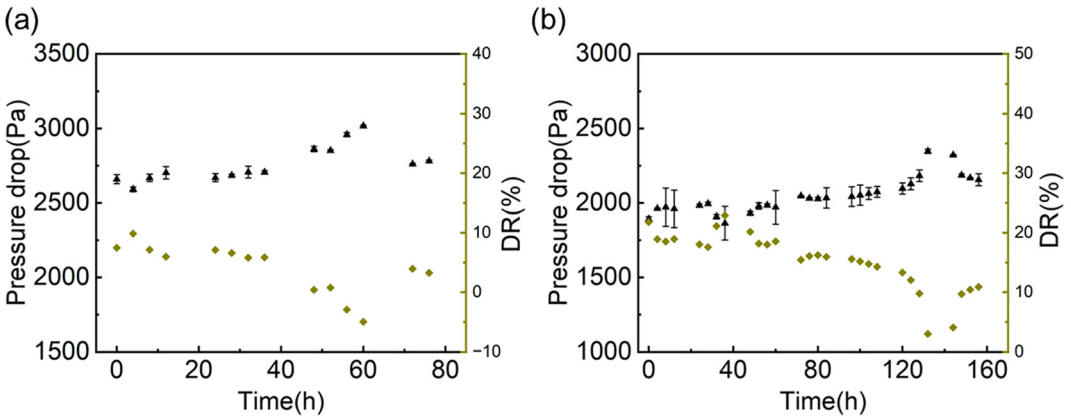

Fig. 7 (a) Hydrodynamic durability test shows the change in the pressure drop (left axis) and drag reduction coefficient (right axis) over time for the hydrophobic slippery liquid-like surface. The drag reduction reduced below 0 at 56 h. (b) Hydrodynamic durability test shows the change in pressure drop (left axis) and drag reduction (right axis) over time for the hydrophilic slippery liquid-like surface. The drag reduction remained around 10% after 1 week.

microchannel.[54–59] Our results suggest that liquid-like surfaces, regardless of their wettability, have much better durability compared to SHSs and SLIPSs. The possible cause of the degradation of liquid-like surfaces under liquid flow could be the loss of flexible polymers with time. To further increase the durability of liquid-like surfaces, the multi-point grafting method (*i.e.*, one flexible polymer will be grafted to the substrate *via* several grafting points) can be employed in the future to reduce flexible polymer loss.[88–92]

4. Conclusion

This study represents the first demonstration of the significant potential of slippery liquid-like surfaces for drag reduction and their outstanding durability. The drag reduction coefficient could reach as high as 20%. Our experimental results also highlighted the effectiveness of slippery liquid-like surfaces in maintaining a stable, low-friction interface that significantly diminished the overall drag force experienced by the fluid. The comparison with SHSs and SLIPSs revealed the distinct advantages of slippery liquid-like surfaces. While SHSs and SLIPSs have shown impressive drag reduction capabilities, their long-term durability issue presents a considerable challenge for practical applications. In contrast, slippery liquid-like surfaces provide a more robust and reliable solution, making them highly suitable for a wide range of microfluidic applications, including those in biomedical devices and energy conversion technologies. For example, in microfluidic energy devices (*e.g.*, electrokinetic energy converters), drag reduction can improve liquid transport and thus enhance the energy conversion efficiency.[93–96] In microfluidic biomedical devices, drag reduction can improve blood circulation, aiding the treatment of cardiovascular diseases.[97] The findings of this study contribute to the fundamental understanding of fluid dynamics over novel slippery liquid-like surfaces and open new avenues for the design and optimization of high-performance microfluidic devices. They will also trigger the interest of broad research communities in this direction to push it moving forward. To facilitate the utilization of slippery liquid-like surfaces in flow applications, future research will focus on systematic fundamental understanding of the mechanism of drag reduction and surface degradation of liquid-like surfaces, effects of the design factors of liquid-like surfaces on their drag reduction performance to optimize the surface design, their drag reduction performance in the turbulent flow regime, large-scale surface fabrication, and further improvement of slippery liquid-like surface durability. The insights gained from this work will be instrumental in advancing the field of drag reduction and pave the way for innovative solutions to improve the performance of broad microfluidic technologies.

Author contributions

H. L. and B. F. conceived the ideas. The experiments were mainly performed by H. L. All authors contributed to the analysis and interpretation of the results and the writing of the paper.

Data availability

Data for this article are available at Dryad at **https://datadryad.org/stash/share/MiFUYDWs51WXmrBpTqh1ck3HwdDJzM1hnkCEbgs2NWw**.

Conflicts of interest

There are no conflicts to declare.

Acknowledgements

The authors are grateful for the support from the National Science Foundation (NSF CBET 2202688) and the Michigan State University for the start-up funding.

References

1 The Study of Drag Reduction on Ships Inspired by Simplified Shark Skin Imitation - Ibrahim - 2018 - Applied Bionics and Biomechanics - Wiley Online Library. **https://onlinelibrary.wiley.com/doi/full/10.1155/2018/7854321** (accessed 2024-09-02).

2 V. Stenzel, Y. Wilke and W. Hage, Drag-Reducing Paints for the Reduction of Fuel Consumption in Aviation and Shipping, *Prog. Org. Coat.*, 2011, **70**(4), 224–229, DOI: **10.1016/j.porgcoat.2010.09.026**.

3 W. N. Felder, G. A. Dale, C. Cash and M. Chang, Prospects for the Application of Practical Drag Reduction Technologies to Legacy Transport Aircraft, in *55th AIAA Aerospace Sciences Meeting*, American Institute of Aeronautics and Astronautics. DOI: **10.2514/6.2017-0044**.

4 J. F. Morrison, 7 - MEMS Devices for Active Drag Reduction in Aerospace Applications, in *MEMS for Automotive and Aerospace Applications*, ed. M. Kraft and N. M. White, Woodhead Publishing Series in Electronic and Optical Materials, Woodhead Publishing, 2013, pp. 153–176. DOI: **10.1533/9780857096487.2.153**.

5 H. Pakzad, A. Nouri-Borujerdi and A. Moosavi, Drag Reduction Ability of Slippery Liquid-Infused Surfaces: A Review, *Prog. Org. Coat.*, 2022, **170**, 106970, DOI: **10.1016/j.porgcoat.2022.106970**.

6 W. Gong, J. Shen, W. Dai, K. Li and M. Gong, Research and Applications of Drag Reduction in Thermal Equipment: A Review, *Int. J. Heat Mass Transfer*, 2021, **172**, 121152, DOI: **10.1016/j.ijheatmasstransfer.2021.121152**.

7 M. M. A. El-Azm, S. Z. Kassab and S. A. Elshafie, Experimental and Numerical Study for Turbulent Flow Drag Reduction in District Cooling Systems, *CFD Lett.*, 2014, **6**(3), 113–125.

8 M. A. D. S. Bernardes, *Developments in Heat Transfer*, BoD – Books on Demand, 2011.
9 Research Status of Marine Drag Reduction Technologies. **https://www.tribology.com.cn/en/article/doi/10.16078/j.tribology.2015.04.020** (accessed 2024-10-12).
10 M. Ahmadzadehtalatapeh and M. Mousavi, A Review on the Drag Reduction Methods of the Ship Hulls for Improving the Hydrodynamic Performance, *Int. J. Marit. Technol.*, 2015, **4**, 51–64.
11 Z. Yan, M. Li, Z. Du, X. Yang, Y. Luo, X. Chen and B. Han, Study on a Tracked Amphibious Robot Bionic Fairing for Drag Reduction, *Ocean Eng.*, 2023, **267**, 113223, DOI: **10.1016/j.oceaneng.2022.113223**.
12 J. Jing, Y. Guo, R. Karimov, J. Sun, W. Huang, Y. Chen and Y. Shan, Drag Reduction Related to Boundary Layer Control in Transportation of Heavy Crude Oil by Pipeline: A Review, *Ind. Eng. Chem. Res.*, 2023, **62**(37), 14818–14834, DOI: **10.1021/acs.iecr.3c02212**.
13 L. P. Chamorro, R. E. A. Arndt and F. Sotiropoulos, Drag Reduction of Large Wind Turbine Blades through Riblets: Evaluation of Riblet Geometry and Application Strategies, *Renewable Energy*, 2013, **50**, 1095–1105, DOI: **10.1016/j.renene.2012.09.001**.
14 Z. Wang, Y. Liu, P. Guo, L. Heng and L. Jiang, Photoelectric Synergetic Responsive Slippery Surfaces Based on Tailored Anisotropic Films Generated by Interfacial Directional Freezing, *Adv. Funct. Mater.*, 2018, **28**(49), 1801310, DOI: **10.1002/adfm.201801310**.
15 K. Han, L. Heng, Y. Zhang, Y. Liu and L. Jiang, Slippery Surface Based on Photoelectric Responsive Nanoporous Composites with Optimal Wettability Region for Droplets' Multifunctional Manipulation, *Adv. Sci.*, 2019, **6**(1), 1801231, DOI: **10.1002/advs.201801231**.
16 K. Han, Z. Wang, L. Heng and L. Jiang, Photothermal Slippery Surfaces towards Spatial Droplet Manipulation, *J. Mater. Chem. A*, 2021, **9**(31), 16974–16981, DOI: **10.1039/D1TA04243B**.
17 C. Shu-man, G. Pu and H. Li-ping, Regulation of Adhesion between Polymer Solid-Liquid Composite Interface and Liquid, *Acta Polym. Sin.*, 2020, **51**(5), 530–547.
18 P. Guo, Z. Wang, X. Han and L. Heng, Nepenthes Pitcher Inspired Isotropic/Anisotropic Polymer Solid–Liquid Composite Interface: Preparation, Function, and Application, *Mater. Chem. Front.*, 2021, **5**(4), 1716–1742, DOI: **10.1039/D0QM00805B**.
19 X. Han, S. Tan, R. Jin, L. Jiang and L. Heng, Noncontact Charge Shielding Knife for Liquid Microfluidics, *J. Am. Chem. Soc.*, 2023, **145**(11), 6420–6427, DOI: **10.1021/jacs.2c13674**.
20 K. Han, Z. Wang, X. Han, X. Wang, P. Guo, P. Che, L. Heng and L. Jiang, Active Manipulation of Functional Droplets on Slippery Surface, *Adv. Funct. Mater.*, 2022, **32**(45), 2207738, DOI: **10.1002/adfm.202207738**.
21 X. Wang, Z. Wang, L. Heng and L. Jiang, Stable Omniphobic Anisotropic Covalently Grafted Slippery Surfaces for Directional Transportation of Drops and Bubbles, *Adv. Funct. Mater.*, 2020, **30**(1), 1902686, DOI: **10.1002/adfm.201902686**.
22 X. Sun, X. Wang, P. Guo, L. Jiang and L. Heng, Photoelectric Synergistic Anisotropic Slippery Interface for Directional Droplets Manipulation, *Nanoscale*, 2023, **15**(35), 14523–14530, DOI: **10.1039/D3NR02779A**.
23 S. Tan, X. Han, Y. Sun, P. Guo, X. Sun, Z. Chai, L. Jiang and L. Heng, Light-Induced Dynamic Manipulation of Liquid Metal Droplets in the Ambient Atmosphere, *ACS Nano*, 2024, **18**(11), 8484–8495, DOI: **10.1021/acsnano.4c00690**.
24 X. Han, R. Jin, Y. Sun, K. Han, P. Che, X. Wang, P. Guo, S. Tan, X. Sun, H. Dai, Z. Dong, L. Heng and L. Jiang, Infinite Self-Propulsion of Circularly On/Discharged Droplets, *Adv. Mater.*, 2024, **36**(18), 2311729, DOI: **10.1002/adma.202311729**.
25 V. Jayaprakash, M. Costalonga, S. Dhulipala and K. K. Varanasi, Enhancing the Injectability of High Concentration Drug Formulations Using Core Annular Flows, *Adv. Healthcare Mater.*, 2020, **9**(18), 2001022, DOI: **10.1002/adhm.202001022**.
26 D. J. Harrison, K. Fluri, K. Seiler, Z. Fan, C. S. Effenhauser and A. Manz, Micromachining a Miniaturized Capillary Electrophoresis-Based Chemical Analysis System on a Chip, *Science*, 1993, **261**(5123), 895–897, DOI: **10.1126/science.261.5123.895**.
27 D. Erickson and D. Li, Integrated Microfluidic Devices, *Anal. Chim. Acta*, 2004, **507**(1), 11–26, DOI: **10.1016/j.aca.2003.09.019**.
28 G. M. Whitesides, The Origins and the Future of Microfluidics, *Nature*, 2006, **442**(7101), 368–373, DOI: **10.1038/nature05058**.
29 Blood viscosity in small tubes: effect of shear rate, aggregation, and sedimentation. DOI: 10.1152/ajpheart.1987.253.3.H540.
30 E. Alinovi and A. Bottaro, Apparent Slip and Drag Reduction for the Flow over Superhydrophobic and Lubricant-Impregnated Surfaces, *Phys. Rev. Fluids*, 2018, **3**(12), 124002, DOI: **10.1103/PhysRevFluids.3.124002**.
31 P. A. Tsai, Slippery Interfaces for Drag Reduction, *J. Fluid Mech.*, 2013, **736**, 1–4, DOI: **10.1017/jfm.2013.376**.
32 M. Liravi, H. Pakzad, A. Moosavi and A. Nouri-Borujerdi, A Comprehensive Review on Recent Advances in Superhydrophobic Surfaces and Their Applications for Drag Reduction, *Prog. Org. Coat.*, 2020, **140**, 105537, DOI: **10.1016/j.porgcoat.2019.105537**.
33 N. J. Shirtcliffe, G. McHale, M. I. Newton and Y. Zhang, Superhydrophobic Copper Tubes with Possible Flow Enhancement and Drag Reduction, *ACS Appl. Mater. Interfaces*, 2009, **1**(6), 1316–1323, DOI: **10.1021/am9001937**.
34 D. Bartolo, F. Bouamrirene, É. Verneuil, A. Buguin, P. Silberzan and S. Moulinet, Bouncing or Sticky Droplets: Impalement Transitions on Superhydrophobic Micropatterned Surfaces, *Europhys. Lett.*, 2006, **74**(2), 299–305, DOI: **10.1209/epl/i2005-10522-3**.
35 P. Tsai, A. M. Peters, C. Pirat, M. Wessling, R. G. H. Lammertink and D. Lohse, Quantifying Effective

Slip Length over Micropatterned Hydrophobic Surfaces, *Phys. Fluids*, 2009, **21**(11), 112002, DOI: **10.1063/1.3266505**.

36 J. P. Rothstein, Slip on Superhydrophobic Surfaces, *Annu. Rev. Fluid Mech.*, 2010, **42**(Volume 42, 2010), 89–109, DOI: **10.1146/annurev-fluid-121108-145558**.

37 S. Gogte, P. Vorobieff, R. Truesdell, A. Mammoli, F. van Swol, P. Shah and C. J. Brinker, Effective Slip on Textured Superhydrophobic Surfaces, *Phys. Fluids*, 2005, **17**(5), 051701, DOI: **10.1063/1.1896405**.

38 C. Ybert, C. Barentin, C. Cottin-Bizonne, P. Joseph and L. Bocquet, Achieving Large Slip with Superhydrophobic Surfaces: Scaling Laws for Generic Geometries, *Phys. Fluids*, 2007, **19**(12), 123601, DOI: **10.1063/1.2815730**.

39 A. Maali and B. Bhushan, Measurement of Slip Length on Superhydrophobic Surfaces, *Philos. Trans. R. Soc., A*, 2012, **370**(1967), 2304–2320, DOI: **10.1098/rsta.2011.0505**.

40 C. Lee, C.-H. Choi and C.-J. Kim, Superhydrophobic Drag Reduction in Laminar Flows: A Critical Review, *Exp. Fluids*, 2016, **57**(12), 176, DOI: **10.1007/s00348-016-2264-z**.

41 M. A. Samaha, F. O. Ochanda, H. V. Tafreshi, G. C. Tepper and M. Gad-el-Hak, In Situ, Noninvasive Characterization of Superhydrophobic Coatings, *Rev. Sci. Instrum.*, 2011, **82**(4), 045109, DOI: **10.1063/1.3579498**.

42 Underwater Sustainability of the "Cassie" State of Wetting, *Langmuir*, 2009, **25**(20), 12120–12126, **https://pubs.acs.org/doi/full/10.1021/la902679c** (accessed 2024-12-02).

43 Y. Xiang, Y. Xue, P. Lv, D. Li and H. Duan, Influence of Fluid Flow on the Stability and Wetting Transition of Submerged Superhydrophobic Surfaces, *Soft Matter*, 2016, **12**(18), 4241–4246, DOI: **10.1039/C6SM00302H**.

44 B. P. Lloyd, P. N. Bartlett and R. J. K. Wood, Active Gas Replenishment and Sensing of the Wetting State in a Submerged Superhydrophobic Surface, *Soft Matter*, 2017, **13**(7), 1413–1419, DOI: **10.1039/C6SM02820A**.

45 D. Saranndhi, D. Chen, J. A. Kleingartner, S. Srinivasan, R. E. Cohen and G. H. McKinley, Sustained Drag Reduction in a Turbulent Flow Using a Low-Temperature Leidenfrost Surface, *Sci. Adv.*, 2016, **2**(10), e1600686, DOI: **10.1126/sciadv.1600686**.

46 J. Breveleri, S. Mohammadshahi, T. Dunigan and H. Ling, Plastron Restoration for Underwater Superhydrophobic Surface by Porous Material and Gas Injection, *Colloids Surf., A*, 2023, **676**, 132319, DOI: **10.1016/j.colsurfa.2023.132319**.

47 Y. Zhao, Z. Xu, L. Gong, S. Yang, H. Zeng, C. He, D. Ge and L. Yang, Recoverable Underwater Superhydrophobicity from a Fully Wetted State via Dynamic Air Spreading, *iScience*, 2021, **24**(12), 103427, DOI: **10.1016/j.isci.2021.103427**.

48 Y. Tuo, H. Zhang, X. Liu and K. Song, Drag Reduction with Different Liquids on Slippery Liquid-Infused Porous Surface, *Surf. Eng.*, 2021, **37**(10), 1215–1222, DOI: **10.1080/02670844.2020.1840757**.

49 L. R. J. Scarratt, L. Zhu and C. Neto, How Slippery Are SLIPS? Measuring Effective Slip on Lubricated Surfaces with Colloidal Probe Atmoc Force Microscopy, *Langmuir*, 2019, **35**(8), 2976–2982, DOI: **10.1021/acs.langmuir.8b03767**.

50 S. Hardt and G. McHale, Flow and Drop Transport Along Liquid-Infused Surfaces, *Annu. Rev. Fluid Mech.*, 2022, **54**(1), 83–104, DOI: **10.1146/annurev-fluid-030121-113156**.

51 C. Vega-Sánchez and C. Neto, Fluid Slip and Drag Reduction on Liquid-Infused Surfaces under High Static Pressure, *Langmuir*, 2024, **40**(8), 4460–4467, DOI: **10.1021/acs.langmuir.3c03792**.

52 M. K. Fu, I. Arenas, S. Leonardi and M. Hultmark, Liquid-Infused Surfaces as a Passive Method of Turbulent Drag Reduction, *J. Fluid Mech.*, 2017, **824**, 688–700, DOI: **10.1017/jfm.2017.360**.

53 L. Ren, H. Hu, L. Bao, N. V. Priezjev, J. Wen and L. Xie, Two Local Slip Modes at the Liquid–Liquid Interface over Liquid-Infused Surfaces, *Phys. Fluids*, 2022, **34**(8), 082017, DOI: **10.1063/5.0098343**.

54 R. Stoddard, K. Nithyanandam and R. Pitchumani, Fabrication and Durability Characterization of Superhydrophobic and Lubricant-Infused Surfaces, *J. Colloid Interface Sci.*, 2022, **608**, 662–672, DOI: **10.1016/j.jcis.2021.09.099**.

55 H. Yan, W. Zhang, Y. Cui, F. Qian, D. Wei, P. Guo, K. Jiao, J. Huang, Q. Wang and C. Zhao, Durable Drag Reduction and Anti-Corrosion for Liquid Flows inside Lubricant-Infused Aluminum/Copper Capillaries, *Chem. Eng. Sci.*, 2023, **266**, 118275, DOI: **10.1016/j.ces.2022.118275**.

56 S. Peppou-Chapman, J. K. Hong, A. Waterhouse and C. Neto, Life and Death of Liquid-Infused Surfaces: A Review on the Choice, Analysis and Fate of the Infused Liquid Layer, *Chem. Soc. Rev.*, 2020, **49**(11), 3688–3715, DOI: **10.1039/D0CS00036A**.

57 A. Sasidharanpillai, Y. Lee and S. Lee, Design of Stable Liquid Infused Surfaces: Influence of Oil Viscosity on Stability, *Colloids Surf., A*, 2022, **646**, 128923, DOI: **10.1016/j.colsurfa.2022.128923**.

58 J. S. Wexler, I. Jacobi and H. A. Stone, Shear-Driven Failure of Liquid-Infused Surfaces, *Phys. Rev. Lett.*, 2015, **114**(16), 168301, DOI: **10.1103/PhysRevLett.114.168301**.

59 C. Vega-Sánchez, S. Peppou-Chapman, L. Zhu and C. Neto, Nanobubbles Explain the Large Slip Observed on Lubricant-Infused Surfaces, *Nat. Commun.*, 2022, **13**, 351, DOI: **10.1038/s41467-022-28016-1**.

60 D. Monga, Z. Guo, L. Shan, S. A. Taba, J. Sarma and X. Dai, Quasi-Liquid Surfaces for Sustainable High-Performance Steam Condensation, *ACS Appl. Mater. Interfaces*, 2022, **14**(11), 13932–13941, DOI: **10.1021/acsami.2c00401**.

61 L. Zhang, Z. Guo, J. Sarma, W. Zhao and X. Dai, Gradient Quasi-Liquid Surface Enabled Self-Propulsion of Highly Wetting Liquids, *Adv. Funct. Mater.*, 2021, **31**(13), 2008614, DOI: **10.1002/adfm.202008614**.

62 J. Sarma, L. Zhang, Z. Guo and X. Dai, Sustainable Icephobicity on Durable Quasi-Liquid Surface, *Chem. Eng. J.*, 2022, **431**, 133475, DOI: **10.1016/j.cej.2021.133475**.

63 L. Zhang, Z. Guo, J. Sarma and X. Dai, Passive Removal of Highly Wetting Liquids and Ice on Quasi-Liquid Surfaces, *ACS Appl. Mater. Interfaces*, 2020, **12**(17), 20084–20095, **https://pubs.acs.org/doi/full/10.1021/acsami.0c02014** (accessed 2024-03-05).

64 H. Vahabi, S. Vallabhuneni, M. Hedayati, W. Wang, D. Krapf, M. J. Kipper, N. Miljkovic, A. Kota and K. Designing Non-Textured, All-Solid, Slippery Hydrophilic Surfaces, *Matter*, 2022, **5**(12), 4502–4512, DOI: **10.1016/j.matt.2022.09.024**.

65 H. Cha, H. Vahabi, A. Wu, S. Chavan, M.-K. Kim, S. Sett, S. A. Bosch, W. Wang, A. K. Kota and N. Miljkovic, Dropwise Condensation on Solid Hydrophilic Surfaces, *Sci. Adv.*, 2020, **6**(2), eaax0746, DOI: **10.1126/sciadv.aax0746**.

66 L. Wang and T. J. McCarthy, Covalently Attached Liquids: Instant Omniphobic Surfaces with Unprecedented Repellency, *Angew. Chem., Int. Ed.*, 2016, **55**(1), 244–248, DOI: **10.1002/anie.201509385**.

67 X. Zhao, B. Khatir, K. Mirshahidi, K. Yu, J. N. Kizhakkedathu and K. Golovin, Macroscopic Evidence of the Liquidlike Nature of Nanoscale Polydimethylsiloxane Brushes, *ACS Nano*, 2021, **15**(8), 13559–13567, DOI: **10.1021/acsnano.1c04386**.

68 A. Y. Fadeev and T. J. McCarthy, Trialkylsilane Monolayers Covalently Attached to Silicon Surfaces: Wettability Studies Indicating That Molecular Topography Contributes to Contact Angle Hysteresis, *Langmuir*, 1999, **15**(11), 3759–3766, DOI: **10.1021/la981486o**.

69 D. Daniel, J. V. I. Timonen, R. Li, S. J. Velling, M. J. Kreder, A. Tetreault and J. Aizenberg, Origins of Extreme Liquid Repellency on Structured, Flat, and Lubricated Hydrophobic Surfaces, *Phys. Rev. Lett.*, 2018, **120**(24), 244503, DOI: **10.1103/PhysRevLett.120.244503**.

70 Y. Huang, Z. Zhang, C. Ma and G. Zhang, Polymer Coating for Antiicing and Deicing, *Polymer*, 2024, **302**, 127047, DOI: **10.1016/j.polymer.2024.127047**.

71 Z. Chai, Z. Teng, P. Guo, Y. He, D. Zhao, X. Zuo, K. Liu, L. Jiang and L. Heng, A Photoelectric Synergistic Flexible Solid Slippery Surface for All-Day Anti-Icing/Frosting, *Small Methods*, 2024, **8**(1), 2400859, DOI: **10.1002/smtd.202400859**.

72 P. Guo, Z. Teng, X. Han, Y. Sun, R. Jin, L. Jiang and L. Heng, Solar-Assisted Solid Slippery Surface for All-Day Ice Free at Extreme-Weather, *Chem. Eng. J.*, 2023, **471**, 144518, DOI: **10.1016/j.cej.2023.144518**.

73 D. Li, L. Ma, B. Zhang and S. Chen, Facile Fabrication of Robust and Photo-Thermal Super-Hydrophobic Coating with Efficient Ice Removal and Long-Term Corrosion Protection, *Chem. Eng. J.*, 2022, **450**, 138429, DOI: **10.1016/j.cej.2022.138429**.

74 S. Tan, X. Han, S. Cheng, P. Guo, X. Wang, P. Che, R. Jin, L. Jiang and L. Heng, Photothermal Solid Slippery Surfaces with Rapid Self-Healing, Improved Anti/De-Icing and Excellent Stability, *Macromol. Rapid Commun.*, 2023, **44**(6), 2200816, DOI: **10.1002/marc.202200816**.

75 H. Agarwal, L. J. Quinn, S. C. Walter, T. J. Polaske, D. H. Chang, S. P. Palecek, H. E. Blackwell and D. M. Lynn, Slippery Anti-Fouling Polymer Coatings Fabricated Entirely from Biodegradable and Biocompatible Components, *ACS Appl. Mater. Interfaces*, 2022, **14**(15), 17940–17949, DOI: **10.1021/acsami.1c25218**.

76 Y. Higaki, M. Kobayashi, D. Murakami and A. Takahara, Anti-Fouling Behavior of Polymer Brush Immobilized Surfaces, *Polym. J.*, 2016, **48**(4), 325–331, DOI: **10.1038/pj.2015.137**.

77 M. Ahlers, A. Buck-Emden and H.-J. Bart, Is Dropwise Condensation Feasible? A Review on Surface Modifications for Continuous Dropwise Condensation and a Profitability Analysis, *J. Adv. Res.*, 2019, **16**, 1–13, DOI: **10.1016/j.jare.2018.11.004**.

78 S. Li, C. W. E. Lam, M. Donati, K. Regulagadda, E. Yavuz, T. Pfeiffer, P. Sarkiris, E. Gogolides, A. Milionis, D. Poulikakos, H.-J. Butt and M. Kappl, Durable, Ultrathin, and Antifouling Polymer Brush Coating for Efficient Condensation Heat Transfer, *ACS Appl. Mater. Interfaces*, 2024, **16**(1), 1941–1949, DOI: **10.1021/acsami.3c17293**.

79 Contact angle hysteresis: a review of fundamentals and applications, *Colloid Polym. Sci.*, 2013, **291**, 247–260, **https://link.springer.com/article/10.1007/s00396-012-2796-6** (accessed 2024-09-02).

80 J. Ou, B. Perot and J. P. Rothstein, Laminar Drag Reduction in Microchannels Using Ultrahydrophobic Surfaces, *Phys. Fluids*, 2004, **16**(12), 4635–4643, DOI: **10.1063/1.1812011**.

81 J. T. R. Watson, R. S. Basu and J. V. Sengers, An Improved Representative Equation for the Dynamic Viscosity of Water Substance, *J. Phys. Chem. Ref. Data*, 1980, **9**(4), 1255–1290, DOI: **10.1063/1.555631**.

82 Y. Zhang, Z. Zhang, J. Yang, Y. Yue and H. Zhang, A Review of Recent Advances in Superhydrophobic Surfaces and Their Applications in Drag Reduction and Heat Transfer, *Nanomaterials*, 2022, **12**(1), 44, DOI: **10.3390/nano12010044**.

83 H. Park, C.-H. Choi and C.-J. Kim, Superhydrophobic Drag Reduction in Turbulent Flows: A Critical Review, *Exp. Fluids*, 2021, **62**(11), 229, DOI: **10.1007/s00348-021-03322-4**.

84 D. Orejon, J. Oh, D. J. Preston, X. Yan, S. Sett, Y. Takata, N. Miljkovic and K. Sefiane, Ambient-Mediated Wetting on Smooth Surfaces, *Adv. Colloid Interface Sci.*, 2024, **324**, 103075, DOI: **10.1016/j.cis.2023.103075**.

85 Z. Liu, T. F. Yap, A. Rajappan, R. A. Shveda, R. M. Rasheed and D. J. Preston, Mitigating Contamination with Nanostructure-Enabled Ultraclean Storage, *Nano Lett.*, 2023, **23**(14), 6315–6322, DOI: **10.1021/acs.nanolett.3c00626**.

86 J. Peng, P. Ye, F. Xu, H. Geng, R. Wang, Y. Jiang, Y. Zhu and H. Wang, Highly Transparent, Durable, and Omniphobic Liquid-like Coatings for Efficient Dynamic de-Wetting and Self-Cleaning Applications, *Chem. Eng. J.*, 2023, **477**, 147090, DOI: **10.1016/j.cej.2023.147090**.

87 F. Chen, D. Boylan, F. Z. Khan, L. Shan, D. Monga, P. E. Zimmern, S. Zhang, K. Palmer and X. Dai, Patterning Bacterial Cells on Quasi-Liquid Surfaces for Biofilm Morphological Control, *Adv. Funct. Mater.*, 2024, **34**(45), 2407099, DOI: **10.1002/adfm.202407099**.

88 H. Park, S. Lim, J. Yang, C. Kwak, J. Kim, J. Kim, S. S. Choi, C. B. Kim and J. Lee, A Systematic Investigation on the Properties of Silica Nanoparticles "Multipoint"-Grafted with Poly(2-Acrylamido-2-Methylpropanesulfonate-Co-Acrylic Acid) in Extreme Salinity Brines and Brine–Oil Interfaces, *Langmuir*, 2020, **36**(12), 3174–3183, DOI: **10.1021/acs.langmuir.9b03692**.

89 M. Artico, C. Roux, F. Peruch, A.-F. Mingotaud and C. Y. Montanier, Grafting of Proteins onto Polymeric Surfaces: A Synthesis and Characterization Challenge, *Biotechnol. Adv.*, 2023, **64**, 108106, DOI: **10.1016/j.biotechadv.2023.108106**.

90 W. K. Ledford and S. M. Kilbey, Impact of Hydrogen Bonding Pendant Groups in Polymer Grafted Nanoparticles on Interlayer Adhesion and Mechanical Properties in Material Extrusion Printing, *Addit. Manuf.*, 2023, **63**, 103419, DOI: **10.1016/j.addma.2023.103419**.

91 Polyvinyl chloride surface coated with polymer brushes using a chain–transfer reaction for enhanced fouling resistance - Almousa - 2024 - Polymers for Advanced Technologies - Wiley Online Library. **https://onlinelibrary.wiley.com/doi/full/10.1002/pat.6208** (accessed 2024-10-18).

92 Y. Niu, X. Bu and X. Zhang, Single Chain Mean-Field Theory Study on Responsive Behavior of Semiflexible Polymer Brush, *Materials*, 2021, **14**(4), 778, DOI: **10.3390/ma14040778**.

93 B. Fan, A. Bhattacharya and P. R. Bandaru, Enhanced Voltage Generation through Electrolyte Flow on Liquid-Filled Surfaces, *Nat. Commun.*, 2018, **9**(1), 4050, DOI: **10.1038/s41467-018-06297-9**.

94 B. Fan and P. R. Bandaru, Modulation of the Streaming Potential and Slip Characteristics in Electrolyte Flow over Liquid-Filled Surfaces, *Langmuir*, 2019, **35**(18), 6203–6210, DOI: **10.1021/acs.langmuir.9b00704**.

95 B. Fan and P. R. Bandaru, Tensorial Modulation of Electrokinetic Streaming Potentials on Air and Liquid Filled Surfaces, *Langmuir*, 2019, **35**(46), 14812–14817, DOI: **10.1021/acs.langmuir.9b02841**.

96 B. Fan and P. R. Bandaru, Possibility of Obtaining Two Orders of Magnitude Larger Electrokinetic Streaming Potentials, through Liquid Infiltrated Surfaces, *Langmuir*, 2020, **36**(34), 10238–10243, DOI: **10.1021/acs.langmuir.0c01771**.

97 G. Li, Y. Sun, X. Zheng, H. J. Choi and K. Zhang, Effect of Drag-Reducing Polymer on Blood Flow in Microchannels, *Colloids Surf., B*, 2022, **209**, 112212, DOI: **10.1016/j.colsurfb.2021.112212**.